Use of CALPUFF to predict airborne Mn levels at schools in an urban area impacted by a nearby manganese alloy plant

Daniel Otero-Pregigueiro[a], Ignacio Fernández-Olmo[a]*

[a] Chemical and Biomolecular Engineering Department, University of Cantabria, Avda. Los Castros s/n, 39005 Santander, Cantabria, Spain

*Corresponding Author

Chemical and Biomolecular Engineering Department, University of Cantabria, Avda. Los Castros s/n, 39005 Santander, Cantabria, Spain

fernandi@unican.es

Declarations of interest: none

Abstract

Children are susceptible to the health effects derived from elevated manganese (Mn) environmental exposure; residents living in urban areas where ferromanganese alloy plants are located are usually exposed to high Mn levels. In this work, a dispersion model developed by the USEPA, CALPUFF, has been used to estimate the airborne Mn levels near educational centers located in Santander bay, Northern Spain, an urban area where high Mn levels have been measured in the last decade. The CALPUFF model was validated in a previous work from a multi-site one-year observation dataset. Air manganese levels in 96 primary, secondary and high schools located in Santander bay were estimated using the CALPUFF model for two months corresponding to warm and cold periods using real meteorological data and Mn emission rates corresponding to different emission scenarios. Results show that when the emission scenario that best represented the observations dataset is used, the air Mn levels exceed the WHO guideline (i.e. 150 ng Mn/m^3) in 24 % and 11 % of the studied schools in the cold and warm periods respectively. These exceedances depend on the distance from the FeMn alloy plant and the direction of the prevailing winds.

Additional emission scenarios based on the implementation of preventive and corrective measures are simulated and analysed in terms of the number of exceedances of the WHO guideline. The age range of children has been also considered in the analysis.

Keywords

Atmospheric manganese; children; school; dispersion modelling; CALPUFF

Air Mn industrial sources

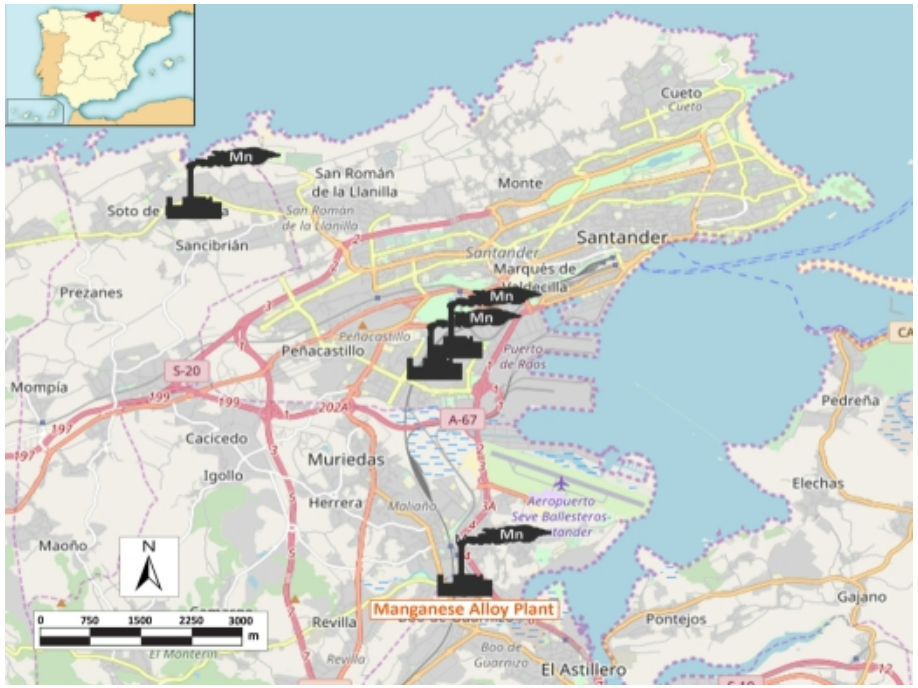

96 SCHOOLS IN THE AREA

CALPUFF MODEL

Simulation of air Mn levels at schools:

reference scenario (S0)

Aplication of abatement measures (alternative scenarios, S1-S4)

Assessment of air Mn concentration at schools

Use of CALPUFF to predict airborne Mn levels at schools in an urban area impacted by a nearby manganese alloy plant

Daniel Otero-Pregigueiro[a], Ignacio Fernández-Olmo[a]*

[a] Chemical and Biomolecular Engineering Department, University of Cantabria, Avda. Los Castros s/n, 39005 Santander, Cantabria, Spain

*Corresponding Author

Chemical and Biomolecular Engineering Department, University of Cantabria, Avda. Los Castros s/n, 39005 Santander, Cantabria, Spain

fernandi@unican.es

Declarations of interest: none

Abstract

Children are susceptible to the health effects derived from elevated manganese (Mn) environmental exposure; residents living in urban areas where ferromanganese alloy plants are located are usually exposed to high Mn levels. In this work, a dispersion model developed by the USEPA, CALPUFF, has been used to estimate the airborne Mn levels near educational centers located in Santander bay, Northern Spain, an urban area where high Mn levels have been measured in the last decade. The CALPUFF model was validated in a previous work from a multi-site one-year observation dataset. Air manganese levels in 96 primary, secondary and high schools located in Santander bay were estimated using the CALPUFF model for two months corresponding to warm and cold periods using real meteorological data and Mn emission rates corresponding to different emission scenarios. Results show that when the emission scenario that best represented the observations dataset is used, the air Mn levels exceed the WHO guideline (i.e. 150 ng Mn/m^3) in 24 % and 11 % of the studied schools in the cold and warm periods respectively. These exceedances depend on the distance from the FeMn alloy plant and the direction of the prevailing winds.

Additional emission scenarios based on the implementation of preventive and corrective measures are simulated and analysed in terms of the number of exceedances of the WHO guideline. The age range of children has been also considered in the analysis.

Keywords

Atmospheric manganese; children; school; dispersion modelling; CALPUFF

1. Introduction

The exposure to moderate/high levels of the metal(loid)s present in the atmosphere is of concern due to adverse health effects derived from their character (e.g. carcinogen, neurotoxic, etc). Although a considerable contribution to the total metal(loid) emission is from natural origin, the anthropogenic emission of these pollutants is much higher in urban and industrial areas (Snyder et al., 2009). Iron and steel industry and the nonferrous metallurgy are reported to be the most intensive airborne and land pollution sources of the metal(loid)s (Hagelstein, 2009). For example, in 2003, the metals industry was the largest source of metal air toxics in the US followed by the electric power industry (Hagelstein, 2009). An environmental assessment of the iron and steel production performed by Strezov and Chaudhary (2017) revealed most significant contribution of manganese (Mn), followed by titanium (Ti), zinc (Zn), chromium (Cr) and lead (Pb). Moreover, Mn alloy production plants are the major source of air Mn (USEPA, 1984).

Although Mn is an essential and abundant micronutrient required for normal development and growth (Erikson and Aschner, 2003; Erikson *et al.*, 2005; Nielsen, 1999), excessive and prolonged inhalation of Mn particulates results in its accumulation in selected brain regions that causes central nervous system (CNS) dysfunctions and an extrapyramidal motor disorder, referred to as manganism (Martin, 2006). Prolonged and chronic exposure to Mn represents a risk factor Parkinson's disease (Gorell *et al.*, 1999). Different studies reported that inhalation is the most hazardous route of Mn exposure; airborne Mn directly enters the organism being

absorbed very effectively (Andersen *et al.*, 1999; Krachler *et al.*, 1999; Mergler *et al.*, 1999).

Since Mn is neurotoxic and considering that the brain and central nervous system are developed in the early years of life, the exposure to Mn may cause neurotoxic effects of particular concern in infants and children (Menezes-Filho et al., 2011; Rodríguez-Barranco et al., 2013). Exposure to environmental Mn in utero has also been associated with decreased neurocognitive and neuro-motor functions (Takser *et al.*, 2004). Recent studies on children and infants have shown the association of Mn exposure with neurotoxic disorders, including motor, behavioral and cognitive deficits (Carvalho *et al.*, 2014; Crossgrove and Zheng, 2004; Mora *et al.*, 2015; Riojas-Rodríguez *et al.*, 2010; Rodríguez-Barranco *et al.*, 2013). Exposure to airborne Mn in children has been found to be associated with cognitive impairment measured as reduced Intelligence Quotient (IQ) (Menezes-Filho *et al.*, 2011; Riojas-Rodríguez *et al.*, 2010). Since Mn neurotoxicity is known for pyramidal effects in adults and has been related to early Parkinsonism (Lucchini *et al.*, 2007, 2012; Roels *et al.*, 2012), control of motor function may be impaired also in younger individuals after early life exposure.

In the face of the evidence of unhealthy effects as a consequence of environment Mn overexposure, a reference concentration (RfC) of 50 ng/m^3 in the respirable fraction has been established by the U.S. Environmental Protection Agency for chronic exposure (US EPA, 1993). The Agency for Toxic Substances and Disease Registry (ATSDR) established a chronic-duration inhalation minimal risk level for Mn of 300 ng/m^3 (ATSDR, 2012). An annual average guideline value of 150 ng/m^3 has also been proposed by the World Health Organization (WHO, 2000). Nevertheless, the Air Quality European Directives (2004/107/EC and 2008/50/EC) only regulate the levels of other metal(loid)s such as As, Cd, Ni and Pb.

Air Mn levels in urban areas have been reported in the literature. Querol *et al.* (2007) reported air Mn concentrations of 4 – 23 ng/m^3 in numerous urban background sites in Spain. Datasets from 15 major cities in Korea over a 16-year time span (1991–2006) were evaluated by Myeong et al. (2009). The mean Mn concentration measured from all the major cities in Korea throughout the entire study period was 71 ng/m^3, while the annual mean values of different cities ranged from 10.5 ng/m^3 in Yeosu (2003) to

615 ng/m^3 in Wonju (2006). The Mn levels were considerably larger in industrialized areas than in other land-use types. The highest Mn concentrations reported in the literature are usually found in the vicinities of ferromanganese alloy plants. For instance, a 24-h Mn concentration of 1,130 ng/m^3 has been reported by Colledge *et al.* (2015) in the Marietta community (Ohio, USA); Haynes *et al* (2010) also reported an annual average concentration of 203 ng/m^3 in the same area. Close to Salvador (Brazil), a 24-h Mn concentration in $PM_{2.5}$ of 151 ng/m^3 was reported by Menezes-Filho *et al.* (2009). Ledoux *et al.* (2006) also reported a 12-h average air Mn concentration of 7,560 ng/m^3 near a ferromanganese alloy plant located in Boulogne-Sur-Mer agglomeration (120,000 inhabitants, France). In addition, several studies have recently reported high levels of air Mn in the vicinity of a manganese alloy plant in the Region of Cantabria, northern Spain: Moreno *et al.* (2011) reported an annual average value of 166 ng/m^3 in the capital of this region, Santander, in the year 2007. Moreover, in Maliaño, a small town where the ferroalloy plant is placed, annual average levels of 781 and 1,072 ng/m^3 were reported in 2005 and 2009 respectively (CIMA, 2006; 2010). A maximum monthly value of 713.9 ng/m^3 was still measured in the same town in 2015 (Hernández-Pellón and Fernández-Olmo, 2016).

A useful way for assessing the exposure to metal(loid)s in the atmosphere is the use of dispersion models in order to provide an integrated understanding of the phenomena that take place (Chen *et al.*, 2012). Furthermore, dispersion models are an essential instrument to develop abatement strategies that can help effectively reduce the levels of the metal(loid)s. Only a few studies have modelled the concentrations of air Mn: Haynes *et al.* (2010), Colledge *et al.* (2015) and Fulk *et al.* (2016) modelled the exposure to air Mn levels through the AERMOD model while Carter *et al.* (2015) simulated atmospheric Mn deposition using the SCIPUFF model. Industrial emission data for particulate-bound metals required to run these models have low confidence ratings since metal emissions are usually estimated on worst-case emission factors, and sometimes not reported (Hagelstein, 2009). The metal industry database quality is uncertain since most of the emission inventories are not representative of site conditions and operations (Hagelstein, 2009). In a recent study, a day-by-day Mn emission inventory depending on the operating conditions of a ferromanganese plant

was developed to run the CALPUFF model to estimate the Mn levels in Santander bay (Otero-Pregigueiro *et al.*, 2018). This model showed a reasonable agreement between observations and Mn modelled values in four sites close to the ferroalloy plant. Unlike AERMOD, CALPUFF is a non-steady-state puff model, and it is recommended for certain near-field applications involving complex terrain and meteorological conditions (Scire *et al.*, 2000). For example, CALPUFF is capable of tracking the puff emitted before, during and after wind shifts and reversals (Burger, 2004), allowing to take into account the wind direction changes that typically occur in the summertime in Santander bay.

Taking into account that children are the most sensitive group to Mn environmental exposure, the large time they spend at school, and the high levels of Mn measured in the last years in Santander bay, the aim of this study is to evaluate the outdoor air Mn concentration in the educational centers existing along this bay using the CALPUFF dispersion model that was previously validated with a large experimental dataset (Otero-Pregigueiro *et al.*, 2018). In addition, alternative emission scenarios corresponding to the potential application of preventive and corrective measures in the main Mn industrial source (i.e. the manganese alloy plant), and also considering the Mn emissions from other minor industrial sources, are evaluated using CALPUFF modelling, as a preliminary approach to estimate the exposure to one of the most susceptible population groups, corresponding to infants, children and adolescents.

2. Methodology

2.1. Site description

The study is focused on the Region of Cantabria, northern Spain, more precisely in Santander bay (Figure 1). Main land uses are residential, industrial and commercial. SW and NE are the prevailing wind directions. The main industrial activities taking place in the bay are sources of air Mn, such as a steel plant, two iron foundries and a ferromanganese alloy production plant (see Figure 1). The later one is located in Maliaño, a 10,000 inhabitants town, where high concentrations of Mn in ambient air have been previously reported (Hernández-Pellón and Fernández-Olmo, 2016; Hernández-Pellón *et al.*, 2017). This town is 7 km away from Santander (172,656

inhabitants in 2016), which is the capital of Cantabria and the most populated city of the region.

The ferromanganese alloy production plant produces high carbon ferromanganese (FeMn HC), refined ferromanganese (FeMn MC) and silicomanganese (SiMn) in electrical furnaces with a maximum capacity of 225,000 t/year. Last reported production rate was 131,000 tons in 2015 (Ferroatlántica, 2016). A total of 96 educational centers are located alongside the Santander bay inside a circle of 11 km radius centered at the ferroalloy plant. These schools account for 37,002 students: 23.2 % are infants from 3 to 5 years old; 41.4 % are children from 6 to 11 years old; 26.1 % are teenagers from 12 to 15 years old and 9.3 % are youths from 16 to 17 years old. A detailed list of these educational centers is shown in Table S1. The location of each center, the distance from the manganese alloy plant, and the number of students by age range are also shown in Table S1.

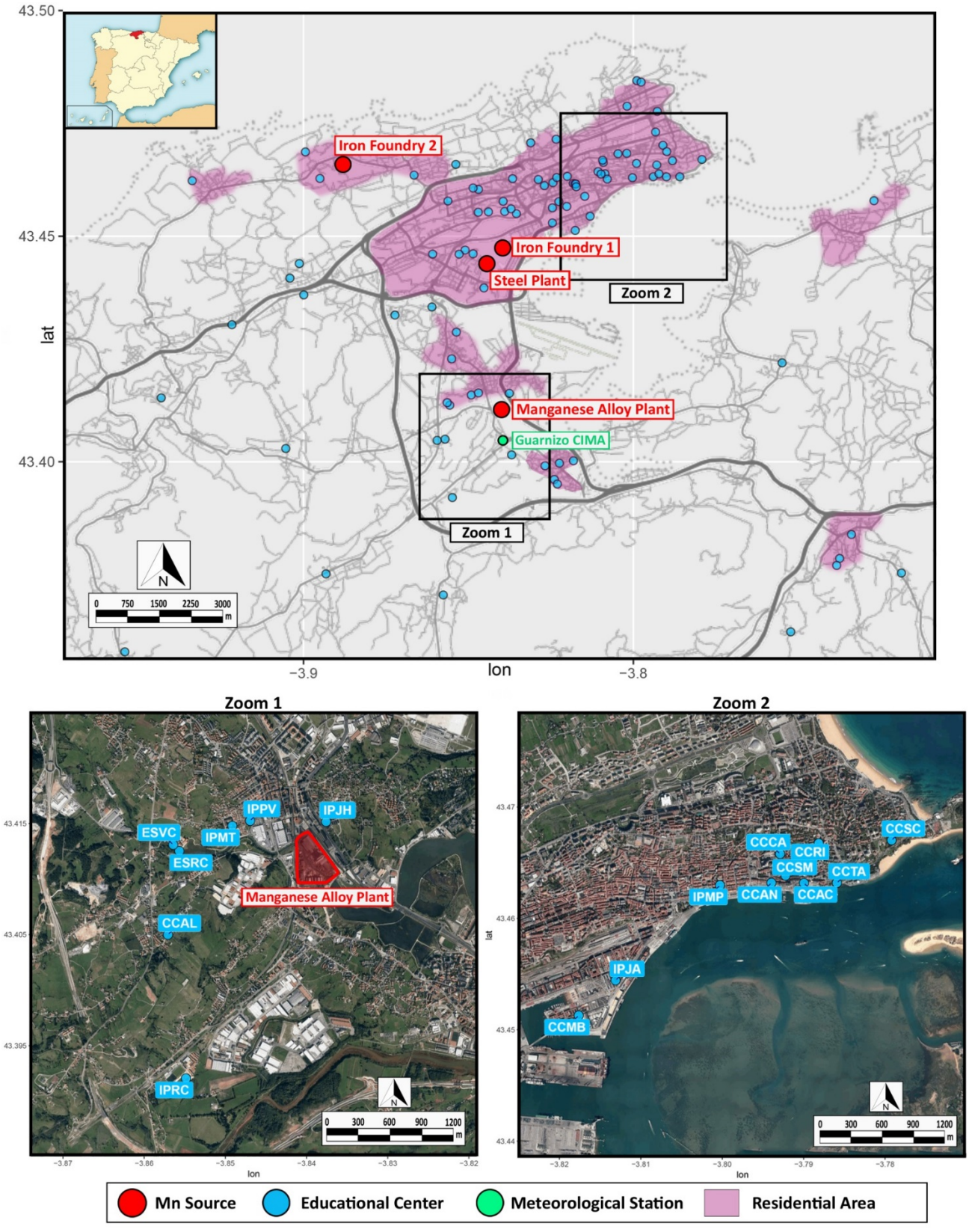

Figure 1: Study area, sources of manganese and educational centers considered in the study. Zoom 1 represents the educational centers in the vicinity of the manganese alloy plant, and zoom 2 the most exposed educational centers in Santander city.

2.2. Model characteristics and setup

In a previous work, we used the CALPUFF model to estimate the PM_{10}-bound Mn concentration alongside the Santander bay; it was validated by comparing the modelled results with a multi-site one-year observation dataset (Otero-Pregigueiro *et al.*, 2018). A detailed description of the Mn emission rate estimation and model characteristics and setup can be found in Otero-Pregigueiro *et al.* (2018). A brief summary is shown below; the Mn emission rates from the Mn industrial sources identified in the studied area (i.e. the manganese alloy plant, the steel plant and the iron foundries) were estimated from emission factors obtained from US EPA (1984); the required information about production rates, energy and raw material consumption, efficiency, and plant characteristics were taken from Environmental Declarations of the companies (Ferroatlántica S.L., 2016; Global Steel Wire S.A., 2015) and Integrated Prevention and Pollution Control (IPPC) permits (BOC, 2008a, 2008b, 2008c, 2008d). A detailed description of the Mn sources and their emissions was only conducted for the ferromanganese alloy plant, which accounted for more than 90 % of the Mn emissions (Otero-Pregigueiro *et al.*, 2018). Emission rate calculations from the other industrial sources (the steel plant and the iron foundries) were simplified because of the low contribution to the total Mn emissions. A single point source was considered for each of these plants. A constant emission rate for the simulated periods was assumed for these industrial sources. The main point and fugitive sources of Mn for the manganese alloy plant are described in Figure 2; the main sections where the Mn emissions can be reduced are highlighted in the figure: first, Mn-bearing particles that are released inside the smelting buildings are not fully collected by the hooding systems, and they are emitted through the wall openings. So, the efficiency of the hooding systems is a key parameter to reduce the Mn fugitive emissions from the smelters. Secondly, ore/slag open storage areas still remain in the plant, leading to fugitive emissions of Mn containing particles. Finally, Mn emissions from non-systematic point sources occur under some operation conditions; in these circumstances, the off-gas exiting the furnaces is directly released through a by-pass pipeline.

CALPUFF is a non-steady-state Lagrangian puff dispersion model that solves the transport, transformation, and removal of pollutants (Scire *et al.*, 2000). Three main components are included in the modelling system: CALMET (a diagnostic 3 – dimensional meteorological model), CALPUFF (an air quality dispersion/deposition model), and CALPOST (a postprocessing package). The USEPA approved version of CALPUFF (v5.8) included in CALPUFF View interface (v8.4.0) has been used in this study. A 20 km x 20 km domain centered in the location of the manganese alloy plant was chosen; the resolution of each cell was 200 m x 200 m.

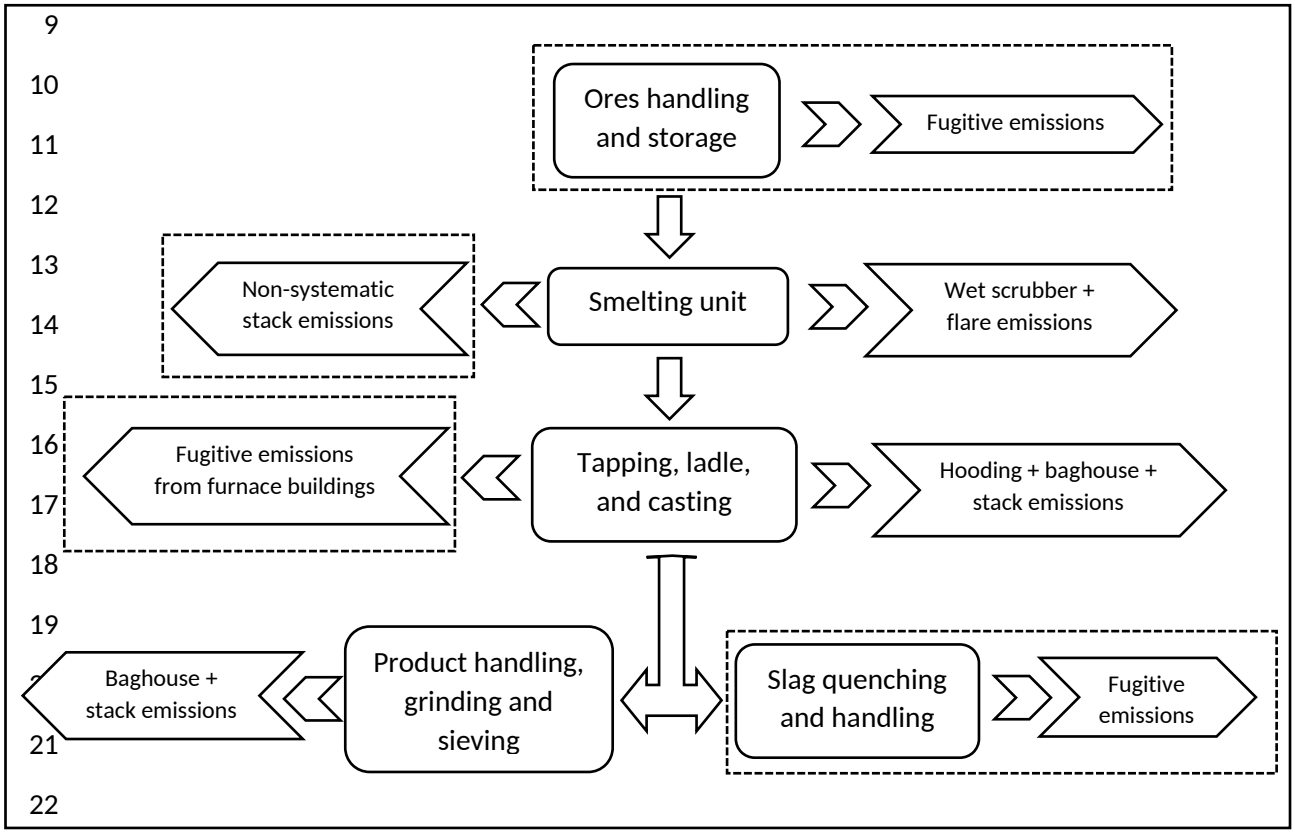

Figure 2. Flow chart of the manganese alloy plant and Mn sources; the sections where Mn emissions can be reduced are highlighted as dotted rectangles (adapted from Otero-Pregigueiro *et al.*, 2018).

Terrain elevation and land cover data were obtained from the Shuttle Radar Topography Mission (SRTM 1) and the Global Land Cover Characterization (GLCC), respectively. Information from the following meteorological stations (see Figure 1) was fed to the model: Parayas AEMET X: 432703 m Y: 4808800 m and Guarnizo CIMA X: 432146 m Y: 4806368 m, for 1-h resolution surface data; and Santander-CMT AEMET X:

435281 m Y: 4815665 m for 1-h resolution surface data and upper-air data from soundings.

2.3. Study design

Because of the high-demanding computing needs of the model, only 2 months were chosen to run the model, one representing the cold period (January) and the other one the warm period (June). This can supply an understanding of the global behavior of the Mn exposure through the entire year. The meteorological data needed to run the model were taken from observations of January and June 2015; according to previous analyses of wind roses in the studied area (Fernández-Olmo *et al.*, 2015; Ruiz *et al.*, 2014), they represent prevailing wind conditions in cold and warm periods in Santander bay. Thus, moderate S/SW wind blows in cold periods while SW winds in the night and morning followed by NE breezes in the afternoon are characteristics in the summertime (see Figure 3).

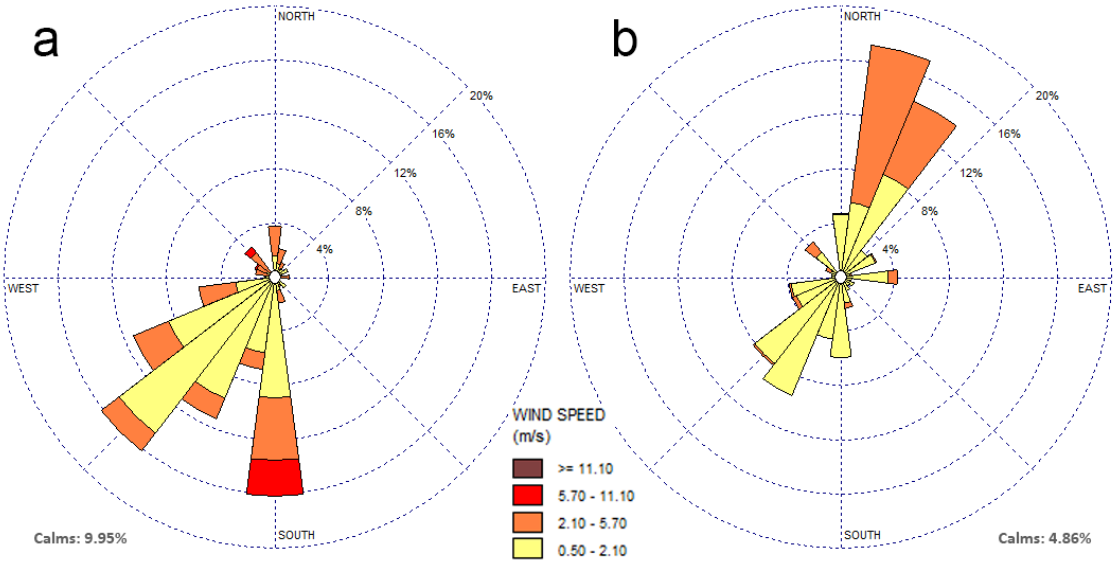

Figure 3. Wind plots for the cold (a) and warm periods (b) in Guarnizo CIMA station: hourly wind data correspond to January 2015 (cold) and June 2015 (warm)

The Mn emission rates were calculated for every simulated days from the emissions of the steel plant, the iron foundries and the manganese alloy plant. Taking into account

that the later one contributed to more than 90 % of Mn emissions in the studied area, different emission scenarios for the ferroalloy plant were considered: the reference scenario based on the emissions that best represented the observations dataset that were assessed in Otero-Pregigueiro *et al*. (2018) and additional scenarios based on the implementation of potential preventive and corrective measures (see Table 1). The reference emission scenario (S0) considered a hooding efficiency inside the smelters of 96 %, a 50 % of piles surface area not covered and no particulate matter control in the off-gas by-pass pipeline (Otero-Pregigueiro *et al*., 2018). The additional scenarios focus on the sections where Mn emissions can be strongly reduced: i) Improving the hooding efficiency in furnace buildings, from 96% to 98%. ii) Reducing the fugitive emissions from ore/slag storage and handling, covering a 90% of the ore/slag storage surface area. iii) Installing high-efficiency control devices (99%) for particulate matter in the by-pass pipeline. In summary, S1 scenario considers the application of the three abatement measures at the same time (98 % of hooding efficiency, 10 % of open piles area, and 99 % of efficiency in the by-pass pipeline), while S2-S4 take into account the application of these measures individually: S2, 99 % of efficiency in the by-pass pipeline; S3, 98 % of hooding efficiency; S4, 10 % of open piles area.

Table 1: Emission scenarios

Scenario	Hooding Efficiency (%)	Open piles area (%)	By-pass pipeline Efficiency (%)
S0 (ref)	96	50	0
S1	98	10	99
S2	96	50	99
S3	98	50	0
S4	96	10	0

2.4. Performance and evaluation analysis

CALPUFF outputs are daily and monthly Mn concentration averages at each receptor site (school). Since WHO guideline value is based on an annual average, monthly values could not be directly contrasted with this guideline value; however, they are compared to have a conservative estimation of the percentage of schools/students that might exceed the WHO value under the chosen meteorological conditions. This analysis is further applied to assess how the potential abatement measures can reduce the Mn

exposure in the studied educational centers. In addition, graphical polar diagrams showing the spatial distribution of the schools and the range of Mn levels are plotted to help with the discussion of the effectiveness of the proposed abatement measures.

3. Results and Discussion

3.1. Modelled PM_{10}-bound Mn concentrations at the selected educational centers

Daily Mn concentrations were calculated at each educational center in both cold and warm periods and monthly averages were calculated at each center for both periods. The statistics of modelled monthly PM_{10} bound Mn concentrations are shown in Table 2: the geometric mean, standard deviation, median, maximum and minimum Mn concentrations were calculated from the monthly values simulated at the 96 educational centers.

Table 2 shows that higher mean, median and maximum values are predicted in the cold period for all the studied scenarios. As shown in Figure 1, most of the schools in the domain are located NE of the ferromanganese alloy plant; since the prevailing wind directions in the wintertime are S and SW (see Figure 3), the Mn plume moves towards these educational centers. In the warm period, when NE wind is blowing the concentration of Mn is lower in these centers. For the reference scenario (S0), the geometric means of the Mn monthly concentrations are 76 and 53 ng/m^3 for the cold and warm periods, respectively (ranges of 1.9-4,401 and 8.1-2,919 ng/m^3). Few simulation studies have reported the levels of air Mn near industrial sources, most of them conducted in Marietta, Ohio (US), where the largest Mn alloy production plant in the US is located. AERMOD has been used to model the air Mn concentration in Marietta (Haynes *et al.*, 2010; Bowler *et al.*, 2012; Colledge *et al.*, 2015; Fulk et *al.*, 2016). An annual average air Mn concentration of 130 ng/m^3 (range of 10-18,130 ng/m^3) was estimated by Haynes *et al.* (2010) from the levels modelled at different residences of more than 100 participants; the authors feed the AERMOD model with 9 Mn emission sources (the FeMn plant contribution was 73 % in 2006). Similar values were reported by Bowler *et al.* (2012) using 2001 Mn emission data averaging the Mn concentration for the period 1991-1995: 180 ng/m^3 (range of 40-960 ng/m^3).

Table 2: Statistics of modelled monthly PM_{10}-bound Mn concentrations at the selected educational centers (geometric mean, standard deviation, median, maximum and minimum) and percentage of centers exceeding the WHO guideline (150 ng/m^3) for each studied scenario (n=96).

	Cold period						**Warm period**					
Scenario	Mean (ng/m^3)	Standard deviation (ng/m^3)	Median (ng/m^3)	Minimum (ng/m^3)	Maximum (ng/m^3)	% of centers exceeding 150 ng/m^3	Mean (ng/m^3)	Standard deviation (ng/m^3)	Median (ng/m^3)	Minimum (ng/m^3)	Maximum (ng/m^3)	% of centers exceeding 150 ng/m^3
S0	76	451	81	2	4,401	24	53	305	51	8	2,919	11
S1	37	149	39	1	1,429	9	26	92	27	4	842	6
S2	74	448	79	2	4,382	24	52	304	51	8	2,906	11
S3	50	366	54	1	3,595	14	35	262	34	5	2,547	9
S4	65	238	67	1	2,256	22	45	141	44	7	1,226	9

The same research group reported later a more detailed study using also AERMOD, distinguishing between total suspended particles (TSP), PM10 and PM2.5 (Colledge *et al.*, 2015). An annual geometric mean of 36, 142 and 171 ng/m^3 was estimated at Marietta for PM2.5, PM10 and TSP respectively (maximum values of 338, 1,334 and 1,607 ng/m^3). No emission data were used in this study; a site-surface area emission method was used instead (Colledge *et al.*, 2015). Lower simulated values were reported by Fulk *et al.* (2016) in the same area; a mean Mn annual value of 16.74 ng/m^3 was obtained in the PM2.5 fraction at 8 km of the main Mn source; a maximum 48-h Mn concentration of 171.84 ng/m^3 was estimated. Colledge *et al.* (2015) also simulate the air Mn levels near a Mn ore processing facility in East Liverpool (Ohio, US). The proximity of this plant to the receptor sites led to higher simulated concentration values; an annual geometric mean of 123 ng/m^3 in PM10 (351 ng/m^3 in TSP) was estimated.

With respect to the effectiveness of the potential abatement measures, the application of all the measures at the same time (S1 scenario) showed a strong reduction in Mn mean, median and maximum concentrations, as expected. The highest reductions were observed at the schools where the maximum monthly Mn concentrations were predicted (IPJH, IPMT, IPPV). The application of the abatement measures individually shows that the most effective measure to reduce the Mn concentration at the studied schools is to increase the hooding efficiency in the smelting buildings (S3 scenario). Some studies reported that although the existing fume capture systems have good capacity, an optimization and upgrading of the hooding system are recommended (Els *et al.*, 2013; Kadkhodabeigi and Haaland, 2013). The reduction of the open storage area (S4 scenario) also leads to diminish the Mn concentration, mainly in the summertime; the arithmetic mean for this scenario is similar to that of S3 scenario in the warm period, but the median is noticeably higher. In most of the selected schools, S3 scenario leads to lower Mn concentrations with respect to S4 scenario; however, the Mn concentrations in IPJH, IPMT and IPPV, which are the schools closest to the ferroalloy plant (see Figure 1, zoom 1) are lower for S4 scenario. This clearly shows that the covering of open storage areas is more effective at the sites closest to the ferromanganese alloy plant. The least efficient control

measure is the installation of a high-efficiency dust control device in the off-gas by-pass pipeline (S2 scenario). Based on observations of the plant operation pattern and the hourly production rate and PM emissions from the main furnaces, a 2-h period per day during working days was assumed for the operation in by-pass mode; in weekends, a 24-h operation in regular mode was assumed. So, the application of this measure leads to a decrease in Mn concentrations in a very short period, barely affecting the daily and monthly averages, as shown in Table 2. However, depending on the weather conditions during the by-pass mode operation, this measure can help in reducing high peak concentrations.

Table 2 also shows the percentage of educational centers where the monthly averages exceed the WHO guideline value (150 ng/m^3). In the reference scenario, the guideline value is exceeded in 24 and 11 % of the studied centers in cold and warm periods respectively. As discussed earlier, the wind conditions registered in the wintertime lead to higher Mn concentrations at the majority of the selected schools. An intermediate percentage of exceedances is expected for the whole year. A relatively high number of schools in Santander bay are located in areas where annual Mn concentrations are expected to exceed the WHO annual guideline value, and taking into account the effects of Mn on children, adolescents and youths, the application of abatement measures are strongly recommended. Thus, the percentage of schools exceeding 150 ng/m^3 can be reduced to 9% and 6% in cold and warm periods respectively if all the potential abatement measures are applied by the ferroalloy plant (S1 scenario).

3.2. Spatial distribution of the PM_{10}-bound Mn concentrations

A polar diagram representing the Mn monthly concentrations at schools for the reference (S0) and the most effective scenario (S1) for the cold and warm periods is plotted in Figure 4. This diagram also allows the analysis of the effect of the position of each center and the distance with respect to the manganese alloy plant on the modelled Mn concentrations. The current scenario (S0) shows higher Mn modelled concentrations at the schools located near the ferroalloy plant (less than 2.5 km); the highest Mn modelled concentrations are found in IPJH: 4,401 and 2,919 ng/m^3 at cold

and warm periods respectively. This school is located some 500 m from the plant. In a previous campaign, a monthly Mn average concentration of 713.9 ng/m^3 and a maximum daily concentration of 3,204 ng/m^3 were measured in IPJH in August 2015 (Hernández-Pellón and Fernández-Olmo, 2016); this site was not used to assess the CALPUFF model developed in our previous work (Otero-Pregigueiro *et al*., 2018), because the only available site to place the sampler did not fulfill all the requirements for microscale siting (the flow around the inlet sampling probe was partially restricted by one of the buildings of this school). So, the measured Mn concentrations at IPJH were probably underestimated.

In the wintertime, a high number of schools located in the first sector (NNE) in the Santander city exceed 150 ng/m^3 (see yellow and light brown circles in figure 4(a)). The Mn concentration at these centers is considerably reduced in the summertime, due to the change in the wind pattern. Figure 3 shows that the contribution from the SW winds in the warm period is much lower than that of the cold period. The influence of the distance from the Mn source and the wind patterns on the Mn levels has been studied in the literature by means of experimental campaigns and also by modelling approaches. Thus, Menezes-Filho *et al*. (2009) found that Mn exposure of children living in the vicinity of a ferroalloy plant 30 km from the city of Salvador (Brazil) was significantly associated with distance and position of their houses relative to wind direction; similar results were found by Lucas *et al*. (2015) in Bagnolo Mella (northern Italy) and by Menezes-Filho *et al*. (2016) in Salvador in the vicinity of ferromanganese plants, where manganese concentration in outdoor dust was inversely related with distance from the plant.

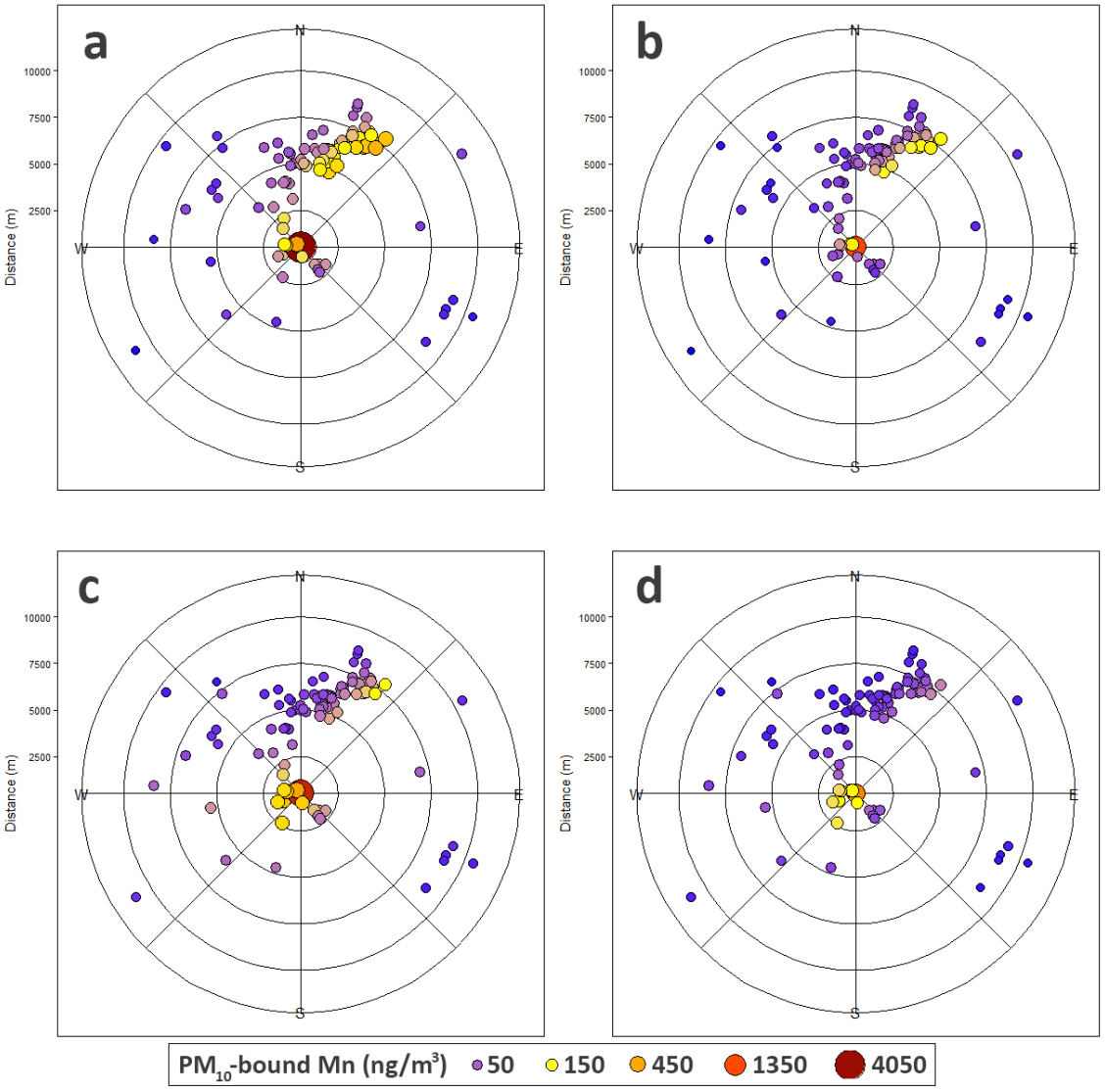

Figure 4: Polar representation of the Mn monthly concentration at schools: a) S0 cold period; b) S1 cold period; c) S0 warm period; d) S1 warm period. The center of the circle represents the location of the manganese alloy plant

With respect to modelling studies, Carter *et al.* (2015) reported the simulated average Mn air concentration in 2006 against the distance from the Mn refinery located in Marietta (Ohio, US) using the SCIPUFF model. The highest simulated Mn levels were about 1,000 ng/m^3 at distances lower than 2.5 km from the refinery. Colledge *et al.* (2015) also reported high simulated Mn levels in the vicinity of Mn sources; in Marietta, sites located between 1.6 and 7.2 km from the FeMn facility were used in the simulation, reaching a maximum annual PM10-bound Mn level of 1,334 ng/m^3

(1,607 ng/m^3 in TSP). Higher annual Mn levels (2,212 ng/m^3 in PM10 and 6,321 ng/m^3 in TSP) were even simulated in East Liverpool, where sites located between 0.08 and 2.1 km from a Mn ore processing facility were used as receptors (Colledge *et al.*, 2015).

The effectiveness of the abatement measures can be observed in Figure 4(b) and 4 (d) for the cold and warm periods respectively. In the wintertime, the reduction of the Mn concentration is mainly observed at schools located in the vicinity of the plant (less than 2.5 km) and in the first sector. The improvement of the Mn exposure at schools located in the first sector is lower in the warm period, but it is better at schools located SW of the plant. The maximum Mn concentrations are again found in IPJH, but they are considerably lower than those simulated in the reference scenario: 1,429 and 842 ng/m^3 in cold and warm periods respectively.

To improve the understanding of the Mn exposure at the schools where the highest concentrations were found, a box plot diagram was built for the 17 most exposed schools, where the median is higher than 150 ng/m^3 either in cold or warm periods (Figure 5). Simulated daily Mn concentrations are represented considering the reference scenario (S0) and the scenario with all the preventive and corrective measures (S1). For each educational center, the maximum, minimum, outliers, 25th, 50th and 75th percentiles of the daily values are represented in this figure. The location of the 17 educational centers are shown in Figure 1: zoom 1 represents the educational centers closest to the manganese alloy plant located in Maliaño, and zoom 2 the most exposed educational centers in Santander city. The schools located in the right-hand side of Figure 5 (from IPJH to ESVC) are those included in zoom 1 while schools in the left-hand side of Figure 5 are in zoom 2 (from CCAC to IPMP). The Mn concentration at schools located in zoom 1 (Maliaño) are lower in the cold period than in warm period with the exception of IPJH, because most of them are located W/SW from the ferroalloy plant, and NE winds in the summertime fumigate the Mn plume towards these schools. Moreover, daily Mn concentration variability is much higher in the cold period because SW wind is blowing during most of the modelled days leading in some cases to low Mn concentrations in receptors located W/SW from the plant.

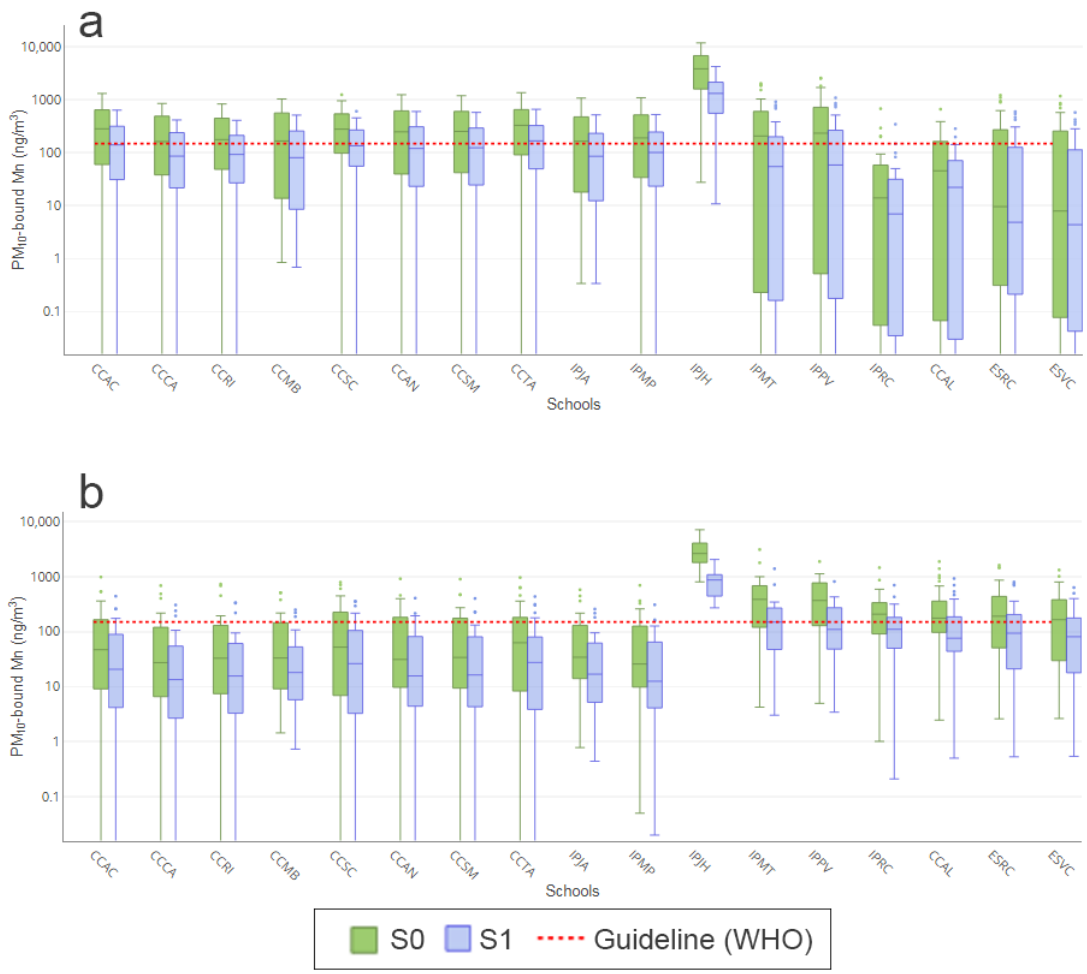

Figure 5: Simulated daily PM_{10}-bound Mn concentration in the most exposed educational centers for the reference scenario (S0) and the scenario with all the preventive and corrective measures (S1): a) Cold period (n=31); b) Warm period (n=30)

On the other hand, the modelled concentrations in schools located in zoom 2 (Santander) are higher in the cold period because of the S/SW prevailing winds; the highest median values are found at the CCAC, CCSC and CCTA sites, located 7-8 km away of the ferroalloy plant, in the eastern part of Santander. The effectiveness of the application of the abatement measures is more clearly observed in schools located in Maliaño (zoom 1) in the warm period: the median of the 7 schools located in Maliaño area was higher than 150 ng/m^3 for the reference scenario; if the measures considered in scenario 1 are applied, the median in 6 of these schools would be lower than 150 ng/m^3. In schools located in Santander (zoom 2), a similar improvement is observed in cold and warm periods when scenario S1 is simulated.

3.3. Analysis of Mn exposure at schools by children age

The age range is often considered when evaluating the exposure of children to air pollutants. For example, air pollution modelling was recently applied to assess the PM_{10} exposure during pregnancy, infancy, childhood and adolescence in the area of Bristol, UK (Gulliver *et al*., 2018). Taking into account that children's cognitive functions and their behavior might be particularly vulnerable to Mn exposure and that this might affect the development of the brain and central nervous system during the first years of live (Elder *et al*., 2006), the age of children is considered in the analysis of Mn exposure. The percentage of students in schools where the WHO guideline was exceeded for the studied age ranges was calculated and is shown in Table 3; results from the five emission scenarios given in Table 1 and two weather conditions (cold and warm periods) are presented.

Table 3: Percentage of students in schools where the WHO guideline (150 ng/m^3) was exceeded by scenario for every age range.

	Age range	n	Scenario				
			S0	**S1**	**S2**	**S3**	**S4**
Cold period	3 - 5	8,574	20	10	20	16	19
	6 - 11	15,312	22	12	22	18	20
	12 - 15	9,668	30	7	30	12	28
	16 - 17	3,448	34	4	34	6	33
Warm period	3 - 5	8,574	11	6	11	9	9
	6 - 11	15,312	12	7	12	10	10
	12 - 15	9,668	13	6	13	10	10
	16 - 17	3,448	12	4	12	7	7

The simulations show that 20% and 11% of infants (from 3 to 5 years) attend schools where Mn concentrations are higher than 150 ng/m^3 in cold and warm periods respectively. This percentage may be reduced to 10% and 6% respectively if all the abatement measures described previously are applied. Children in elementary schools (from 6 to 11 years) is the most populated group (41.4 %); 22% and 12% of this group in cold and warm periods respectively attend schools where Mn levels are higher than 150 ng/m^3; under S1 scenario, they fall to 12% and 7%. Some studies have reported the association of Mn exposure with cognitive effects on children of the same age range: Menezes-Filho *et al*. (2011) reported that highly Mn exposed children (6-12

years) are associated with poorer cognitive performance, especially in the verbal domain. A similar conclusion was obtained by Rodríguez-Barranco *et al*. (2013); a 50 % increase of hair Mn levels would be associated with a decrease of 0.7 points in the IQ of children aged 6-13 years.

The age ranges where higher percentage of exceedances are observed correspond to teenagers (from 12 to 15 years) and youths (from 16 to 17 years). The effectiveness of the application of the proposed abatement measures is higher for these age ranges, mainly in the cold period, due to a higher contribution of these groups at schools located in Santander (zoom 2): the percentage of exceedances is reduced from 30 to 7% (teenagers) and from 34 to 4 % (youths) in the cold period, and from 13 to 6% (teenagers) and from 12 to 4 % (youths) in the warm period. This age range is supposed to be less sensitive to Mn exposure; for example, Torrente *et al*. (2005) did not find an association of hair Mn with cognitive effects on children living in zones of Tarragona (eastern Spain). However, Lucchini *et al*. (2012) did find sub-clinical deficits in olfactory and motor function among adolescents aging 11 to 14 years living in northern Italy, where historical ferromanganese activities were developed.

3.4. Limitations and strengths

The main limitation of the present study is that outdoor PM10-bound Mn was only estimated at the schools' locations, and this may not fully reflect personal children exposure. This was solved in a recent study by Fulk *et al*. (2016) calculating a time-weighted ambient Mn concentration from the simulated values at home (70 %) and school (30 %). In addition, two months representing cold and warm periods and their characteristic wind patterns were simulated in the present study; longer simulation periods are usually used in the literature, since those simulations are more reliable, mainly for chronic exposure studies (Fulk *et al*., 2016). However, because we intended to simulate different emissions scenarios that took into account some abatement strategies, a compromise between the number of runs and the simulation period was taken, based on the overall computational time required to run all the simulations.

Other limitations were associated with the quality of the model. Possible options for model improvements may include the consideration of local-scale phenomena

(canyon-street effects, building downwash, surface dust resuspension, etc), and refinement of the emission inventory by incorporating detailed particle size distribution for each emission source.

Despite these limitations, the model used in this work was developed from a detailed day-by-day Mn emission inventory, including point and fugitive sources. Other studies do not include Mn emission data (Colledge *et al.*, 2015), or fugitive Mn emissions (Fulk *et al.*, 2016). The later authors reported that fugitive emissions from a Mn refinery are generally coarser than PM2.5 and therefore, the impact of these emissions on the PM2.5-bound Mn levels is reduced. However, an important contribution of the Mn fugitive emissions from these facilities is associated with fine particles generated in the smelter buildings that are not fully captured (Hernández-Pellón *et al.*, 2017). A further strength of the model is that it was able to describe a wide air Mn concentration range in accordance with observations (Otero-Pregigueiro et al., 2018). This allows to simulate a wide range of air Mn monthly levels (1.9-4,401 ng/m^3 and 8.1-2,919 ng/m^3 for cold and warm periods, respectively), estimating the Mn levels at schools located between 500 and 10,950 m from the main source. The current study should be considered as a preliminary approach to estimate the Mn exposure for children living in an urban area highly impacted by a manganese alloy plant, and to analyze how this exposure may be reduced by different abatement measures.

4. Conclusions

Air pollution modelling was used to predict the PM10-bound manganese levels at schools located in Santander bay (northern Spain), an urban/industrial area where a ferromanganese alloy plant is operating. The CALPUFF model previously validated with a multi-site dataset was used to simulate the Mn concentration at 96 schools located in Santander bay at distances ranging from 500 to 10,950 m from the ferroalloy plant. The simulations were carried out for cold and warm periods, and for different emission scenarios. The results show that Mn modelled concentrations exceed the WHO guideline (150 ng/m^3) in 24% and 11% of the educational centers for cold and warm periods respectively. The application of potential abatement measures to be applied in the ferromanganese plant would lead to a significant decrease of the mean and

maximum monthly concentrations at schools; among the studied abatement measures, the improvement of the hooding efficiency in furnace buildings is the most effective, followed by the covering of the open ore and slag piles area. The later measure is particularly effective at the schools located in the vicinity of the plant. The distance between the educational centers and the ferroalloy plant dramatically affects the levels of Mn; however, the wind pattern also plays an important role on the modelled Mn concentrations. Thus, the SW winds that typically blow in the wintertime increase the levels of Mn at the schools located in the eastern part of Santander, which is the most populated city in the region, leading to several exceedances of the WHO guideline. In the warm period, the schools closest to the plant located in Maliaño are exposed to higher Mn concentrations because of the shift of the wind direction (SW in the night and morning, and NE in the afternoon); the effectiveness of the simulated abatement measures is higher in the warm period for these schools.

Finally, the age of children potentially exposed to Mn has been assessed. Thus, the simulations show that 20 and 11 % of infants attend schools where Mn concentrations are higher than the WHO guideline in cold and warm periods respectively if no abatement measures are applied. These percentages may be reduced to 10 and 6 % if these measures are implemented. Similar figures are shown for children in elementary schools, which represent more than 40 % of the students considered in the study. The strongest reduction in Mn exceedances is found for teenagers and youths.

Given the evidences reported in the literature reviewed in this work associating high Mn exposure with growth and neurological impairments in children, the results found in this work support that Mn concentrations should be reduced in Santander bay to protect the health of children at schools, mainly in the first age ranges, infants (3-5 years) and children (6-11 years). The approach carried out in this work is a useful way to check different preventive and corrective measures to be applied in the study area and elsewhere to reduce the exposure to Mn.

Funding

This work was supported by the Spanish Ministry of Economy and Competitiveness (MINECO) through the CTM2013-43904R Project. This funding source was not involved

in the study design; data collection, analysis, or interpretation; the writing of the article; or the decision to submit for publication.

Conflict of interest

The authors have no competing interest to declare

Acknowledgments

The authors acknowledge the Spanish State Meteorology Agency (AEMET) for providing meteorological and atmospheric sounding data for the period of study.

References

Andersen, M., Gearhart, J., Clewell, H., 1999. Pharmacokinetic data needs to support risk assessments for inhaled and ingested manganese, Neurotoxicology, 20(2–3), 161–171.

ATSDR (Agency for Toxic Substances and Disease Registry), 2012. Toxicological profile for manganese. Atlanta, GA: U.S. Department of Health and Human Services, Public Health Service.

BOC, 2008a. Autorización Ambiental Integrada: Ferroatlántica S.L., Boletín Oficial Cantabria 107. 7569-7582

BOC, 2008b. Autorización Ambiental Integrada: Global Steel Wire S.A., Boletín Oficial Cantabria, 125, 8967–8977.

BOC, 2008c. Autorización Ambiental Integrada: Industrias Hergom S.A., Boletín Oficial Cantabria, 248, 17477–17488.

BOC, 2008d. Autorización Ambiental Integrada: Saint-Gobain Canalización S.A., Boletín Oficial Cantabria, 142, 9965-9974.

Burger, L. W., 2004. Hexavalent chromium air dispersion modelling in the South African ferrochromium industry. Proceedings of the Tenth International Ferroalloys Congress, Cape Town, South Africa, 806–817.

Carter, M.R., Gaudet, B.J., Stauffer, D.R., White, T.S., Brantley, S.L., 2015. Using soil records with atmospheric dispersion modeling to investigate the effects of clean air regulations on 60 years of manganese deposition in Marietta, Ohio (USA). Sci. Total Environ. 515–516, 49–59.

Carvalho, C.F., Menezes-Filho, J.A., de Matos, V.P., Bessa, J.R., Coelho-Santos, J., Viana, G.F.S., Argollo, N., Abreu, N., 2014. Elevated airborne manganese and low executive function in school-aged children in Brazil, Neurotoxicology, 45, 301–308.

Chen, B., Stein, A.F., Castell, N., de la Rosa, J. D., Sanchez de la Campa, A.M., Gonzalez-Castanedo, Y., Draxler, R.R., 2012. Modeling and surface observations of arsenic dispersion from a large Cu-smelter in southwestern Europe. Atmos. Environ. 49, 114–122.

CIMA. Government of Cantabria, 2006. Evaluación de la influencia de la dirección del viento en el manganeso contenido en la fracción PM10 en Alto Maliaño. Internal Report C- 098/2004.4.

CIMA, Government of Cantabria, 2010. Evaluación de la calidad del aire y analítica de metales en la fracción PM10 en el Alto Maliaño. Internal Report C-077/2008.

Colledge, M. A., Julian, J.R., Gocheva, V.V., Beseler, C.L., Roels, H.A., Lobdell, D.T., Bowler, R.M., 2015. Characterization of air manganese exposure estimates for residents in two Ohio towns. J. Air Waste Manag. Assoc. 28(10), 1304–1314.

Crossgrove, J., Zheng, W., 2004. Manganese toxicity upon overexposure. NMR Biomed. 17(8), 544–553.

Elder, A., Gelein, R., Silva, V., Feikert, T., Opanashuk, L., Carter, J., Potter, R., Maynard, A., Ito, Y., Finkelstein, J., Oberdorster, G., 2006. Translocation of inhaled ultrafine manganese oxide particles to the central nervous system. Environ. Health Perspect. 114, 1172-1178

Els, L., Cowx, P., Nordhagen, R., Kornelius, G., Andrew, N., Smith, P., 2013. Analysis of a ferromanganese secondary fume extraction system to improve design methodologies. The thirteenth International Ferroalloys Congress, 967–978.

Erikson, K.M., Aschner, M., 2003. Manganese neurotoxicity and glutamate-GABA interaction. Neurochem. Int. 43, 475-480.

Erikson, K.M., John, CE, Jones, S.R., Aschner, M., 2005. Manganese accumulation in striatum of mice exposed to toxic doses is dependent upon a functional dopamine transporter. Environ. Toxicol. Pharmacol. 20, 390-394.

Fernández-Olmo, I., Puente, M., Irabien, A., 2015. A comparative study between the fluxes of trace elements in bulk atmospheric deposition at industrial, urban, traffic, and rural sites. Environ. Sci. Pollut. Res. 22 (17), 13427-13441.

Ferroatlántica S.L., 2016. Declaración Ambiental 2015 Centro Productivo: Fábrica de Boo.

Fulk, F., Haynes, E.N., Hilbert, T.J., Brown, D., Petersen, D., Reponen, T., 2016. Comparison of stationary and personal air sampling with an air dispersion model for children's ambient exposure to manganese. J. Expos. Sci. Environ. Epidemiol. 26, 494-502.

Global Steel Wire S.A., 2015. Declaración Ambiental GSW. http://www.globalsteelwire.com/Pdf/productos/DECLARACI%C3%93N%20AMBIENTAL%202015%201S2016.pdf (accessed 23 January 2016).

Gorell, J.M., Johnson, C.C, Rybicki, B.A., Peterson, E.L., Kortsha, G.X., Brown, G.G., Richardson, R.J., 1999. Occupational exposure to manganese, copper, lead, iron, mercury, and zinc and the risk of Parkinson's disease. Neurotoxicology 20, 239-248.

Gulliver, J., Elliott, P., Henderson, J., Hansell, A.L., Vienneau, D., Cai, Y., McCrea, A., Garwood, K., Boyd, A., Neal, L., Agnew, P., Fecht, D., Briggs, D., de Hoogh, K., 2018. Local- and regional-scale air pollution modelling (PM10) and exposure assessment for pregnancy trimesters, infancy, and childhood to age 15 years: Avon Longitudinal Study of Parents And Children (ALSPAC). Environ. Int. 113, 10-19

Hagelstein, K., 2009. Globally sustainable manganese metal production and use. J. Environ. Manage. 90 (12), 3736-3740.

Haynes, E. N., Heckel, P., Ryan, P., Roda, S., Leung, Y.K., Sebastian, K., Succop, P., 2010. Environmental manganese exposure in residents living near a ferromanganese refinery in Southeast Ohio: A pilot study. Neurotoxicology 31(5), 468–474.

Hernández-Pellón, A., Fernández-Olmo, I., 2016. Monitoring the levels of particle matter-bound manganese: An intensive campaign in an urban/industrial area. In: Conference Proceedings 2nd International Conference on Atmospheric Dust - DUST2016. ProScience 3, 50-55.

Hernández-Pellón, A., Fernández-Olmo, I., Ledoux, F., Courcot, L., Courcot, D., 2017. Characterization of manganese-bearing particles in the vicinities of a manganese alloy plant. Chemosphere 175, 411–424.

Kadkhodabeigi, M., Haaland , D., 2013. Design of secondary fume capturing hood for casting hall of a SiMn production plant. The thirteenth International Ferroalloys Congress, 989–998.

Krachler, M., Rossipal, E., Micetic-Turk, D., 1999. Concentrations of trace elements in sera of newborns, young infants, and adults. Biol. Trace Elem. Res. 68(2), 121–35.

Ledoux, F., Laversin, H., Courcot, D., Courcot, L., Zhilinskaya, E.A., Puskaric, E., Aboukaïs, A., 2006. Characterization of iron and manganese species in atmospheric aerosols from anthropogenic sources. Atmos. Res. 82(3–4), 622–632.

Lucas, E.L., Bertrand, P., Guazzetti, S., Donna, F., Peli, M., Jursa, T.P., Lucchini, R., Smith, D.R., 2015. Impact of ferromanganese alloy plants on household dust manganese levels: Implications for childhood exposure. Environ. Res. 138, 279–290.

Lucchini, R.G., Albvini, E., Benedetti, L., Borghesi, S., Coccaglio, R., Malara, E.C., Parrinello, G., Garattini, S., Resola, S., Allessio, L., 2007. High prevalence of Parkinsonian disorders associated to Manganese exposure in the vicinities of ferroalloy industries. Am. J. Ind. Med. 50, 788–800.

Lucchini, R. G., Guazzetti, S., Zoni, S., Donna, F., Peter, S., Zacco, A., Salmistraro, M., Bontempi, E., Zimmerman, N.J., Smith, D.R., 2012. Tremor, olfactory and motor changes in Italian adolescents exposed to historical ferro-manganese emission. Neurotoxicology 33(4), 687–696.

Martin, C.J., 2006. Manganese neurotoxicity: connecting the dots along the continuum of dysfunction. Neurotoxicology 27, 347–349

Menezes-Filho, J.A., Paes, C.R., de C. Pontes, Â.M., Moreira, J.C., Sarcinelli, P.N., Mergler, D., 2009. High levels of hair manganese in children living in the vicinity of a ferro-manganese alloy production plant. Neurotoxicology 30(6), 1207–1213.

Menezes-Filho, J.A., Novaes, C.O., Moreira, J.C., Sarcinelli, P.N., Mergler, D., 2011. Elevated manganese and cognitive performance in school-aged children and their mothers. Environ. Res. 111(1), 156-163.

Menezes-Filho, J.A., Fraga de Souza, K.O., Gomes Rodrigues, J.L., Ribeiro dos Santos, N., De Jesus Bandeira, M., Koin N.L., do Prado Oliveira, S.S., Campos Godoy, A.L.P., Mergler, D., 2016. Manganese and lead in dust fall accumulation in elementary schools near a ferromanganese alloy plant. Environ. Res. 148, 322–329.

Mergler, D., Baldwin, M., Bélanger, S., Larribe, F., Beuter, A., Bowler, R., Panisset, M., Edwards, R., de Geoffroy, A., Sassine, M.P., Hudnell, K., 1999. Manganese neurotoxicity, a continuum of dysfunction: Results from a community based study. Neurotoxicology 20(2–3), 327–342.

Mora, A.M., Arora, M., Harley, K.G., Kogut, K., Parra, K., Hernández-Bonilla, D., Gunier, R.B., Bradman, A., Smith, D.R., Eskenazi, B., 2015. Prenatal and postnatalmanganese teeth levels and neurodevelopment at 7, 9, and 10.5 years in the CHAMACOS cohort. Environ. Int. 84, 39–54.

Moreno, T., Pandolfi, M., Querol, X., Lavín, J., Alastuey, A., Viana, M., Gibbons, W., 2011. Manganese in the urban atmosphere: Identifying anomalous concentrations and sources. Environ. Sci. Pollut. Res. 18(2), 173–183.

Myeong, S., Lee, K.-H., Kim, K.-H., 2009. Airborne manganese concentrations on the Korean peninsula from 1991 to 2006. J. Environ. Manage. 91 (2), 336-343.

Nielsen, FH., 1999. Ultratrace minerals. In: Shils M, editor. Nutrition in Health and disease. Baltimore: Williams & Wilkins, pp. 283–303.

Otero-Pregigueiro, D., Hernández-Pellón, A., Borge, R., Fernández-Olmo, I., 2018. Estimation of PM10-bound manganese concentration near a ferromanganese alloy plant by atmospheric dispersion modelling. Sci. Total Environ. 627, 534–543.

Querol, X., Viana, M., Alastuey, A., Amato, F., Moreno, T., Castillo, S., Pey, J., de la Rosa, J., Sánchez de la Campa, A., Aríñano, B., Salvador, P., García Dos Santos, S., Fernández-Patier, R., Moreno-Grau, S., Negral, L., Minguillón, M.C., Monfort, E., Gil, J.I., Inza, A., Ortega, L.A., Santamaría, J.M., Zabalza, J., 2007. Source origin of trace elements in PM from regional background, urban and industrial sites of Spain. Atmos. Environ., 41(34), 7219–7231.

Riojas-Rodríguez, H., Solís-Vivanco, R., Schilmann, A., Montes, S., Rodríguez, S., Ríos, C., Rodríguez-Agudelo, Y., 2010. Intellectual function in Mexican children living in a mining area and environmentally exposed to manganese. Environ. Health Perspect. 118(10), 1465–1470.

Rodríguez-Barranco, M., Lacasaña, M., Aguilar-Garduño, C., Alguacil, J., Gil, F., González-Alzaga, B., Rojas-García, A., 2013. Association of arsenic, cadmium and manganese exposure with neurodevelopment and behavioural disorders in children: A systematic review and meta-analysis. Sci. Total Environ. 454–455, 562–577.

Roels, H. A., Bowler, R.M., Kim, Y., Henn, B.C., Mergler, D., Hoet, P., Gocheva, V.V., Bellinger, D.C., Wright, R.O., Harris, M.G., Chang, Y., Bouchard, M.F., Riojas-Rodriguez, H., Menezes-Filho, J.A., Téllez-Rojo, M.M., 2012. Manganese exposure and cognitive deficits: A growing concern for manganese neurotoxicity. Neurotoxicology 33(4), 872–880.

Ruiz, S., Fernández-Olmo, I., Irabien, Á., 2014. Discussion on graphical methods to identify point sources from wind and particulate matter-bound metal data. Urban Climate 10, 671–681.

Scire, J. S., Strimaitis, D. G., Yamartino, R. J., 2000. A User ' s Guide for the CALPUFF Dispersion Model. Earth Tech, Inc.

http://www.src.com/calpuff/download/CALPUFF_UsersGuide.pdf (accessed 23 January 2017).

Snyder, D.C., Schauer, J.J., Gross, D.S., Turner, J.R., 2009. Estimating the contribution of point sources to atmospheric metals using single-particle mass spectrometry. Atmos. Environ. 43(26), 4033-4042.

Strezov, V., Chaudhary, C., 2017. Impacts of iron and steelmaking facilities on soil quality. J. Environ. Manage. 203, 1158-1162.

Takser, L., Lafond, J., Bouchard, M., St-Amour, G., Mergler, D., 2004. Manganese levels during pregnancy and at birth: relation to environmental factors and smoking in a Southwest Quebec population. Environ. Res. 95(2):119–25.

Torrente, M., Colomina, M.T., Domingo, J.L., 2005. Metal Concentrations in Hair and Cognitive Assessment in an Adolescent Population. Biol. Trace Elem. Res. 104, 215-221.

US EPA, 1984. Locating and Estimating Sources of Manganese. https://www3.epa.gov/ttnchie1/le/manganes.pdf (accessed 5 March 2015).

US EPA, 1993. Printout of reference concentration (RfC) for chronic inhalation exposure for manganese as verified 9/23/93, dated 12/93.

WHO, World Health Organization, 2000. Air Quality Guidelines for Europe. WHO Regional Publications, European Series (91), 288.

SUPPLEMENTARY MATERIAL

Table S1. List of schools, 2015/2016 academic course*

School	Reference	District	Distance from FeMn plant (m)	UTM X (m)	UTM Y (m)	Degrees from FeMn plant	Students 3 - 5	Students 6 - 11	Students 12 – 15	Students 16 -17
Ángeles Custodios	CCAC	Santander	7200	436094	4812642	35	27	110	118	0
Atalaya	CCAT	Santander	7350	434911	4813221	24	54	140	88	0
Castroverde	CCCA	Santander	7400	435860	4812934	32	254	460	348	65
Centro Social Bellavista Julio Blanco	CCSB	Santander	8600	435389	4815016	22	76	83	65	0
Compañía de María	CCCM	Santander	6500	434418	4812786	21	34	100	116	0
Cumbres	CCCU	Santander	6000	433806	4812500	17	0	128	97	0
Haypo	CCHA	Santander	7200	435363	4812978	28	75	128	92	0
Jardín de África	CCJA	Santander	6900	433399	4813593	11	134	253	180	0
La Anunciación	CCLA	Santander	6400	434588	4812732	23	38	72	0	0
La Salle	CCLS	Santander	5600	433309	4812525	12	174	351	296	128
María Auxiliadora (Salesianos)	CCMA	Santander	6650	434549	4813011	22	207	427	317	65
María Reina Inmaculada	CCRI	Santander	7450	436245	4813038	34	48	113	86	0
Mercedes	CCME	Santander	6000	433663	4812675	15	165	321	180	0
Miguel Bravo - Antiguos Alumnos de la Salle	CCMB	Santander	4800	433843	4811343	21	83	239	107	0
Niño Jesús	CCNJ	Santander	5000	431720	4811822	356	191	0	0	0
Purísima Concepción	CCPC	Santander	5700	434086	4812181	20	57	147	94	0
Sagrado Corazón Esclavas	CCSC	Santander	7900	436969	4813060	38	149	432	327	147
San Agustín	CCSA	Santander	8300	435885	4814255	27	210	481	266	89
San Antonio	CCAN	Santander	6850	435771	4812647	32	0	0	76	0
San José Santander	CCSJ	Santander	6300	434490	4812725	22	96	243	186	53
San Martín	CCSM	Santander	7000	435912	4812717	33	26	115	95	0
Santa María Micaela	CCMM	Santander	5000	432118	4811827	0	105	306	191	0
Tagore	CCTA	Santander	7200	436422	4812640	37	90	0	0	0
Verdemar	CCVE	Santander	6200	429905	4812745	340	180	324	216	0

School	Reference	District	Distance from FeMn plant (m)	UTM X (m)	UTM Y (m)	Degrees from FeMn plant	Students 3 - 5	Students 6 - 11	Students 12 – 15	Students 16 -17
Los Viveros	EILV	Santander	5350	433642	4811936	17	113	0	0	0
Antonio Mendoza	IPAM	Santander	5900	433849	4812490	17	150	237	0	0
Cabo Mayor	IPCB	Santander	8100	435145	4814388	22	185	231	0	0
Cisneros	IPCI	Santander	5950	433869	4812487	17	186	283	0	0
Dionisio García Barredo	IPDG	Santander	6650	434533	4813066	21	53	71	0	0
Elega Quiroga	IPEQ	Santander	4000	431333	4810793	350	170	283	0	0
Eloy Villanueva	IPEV	Santander	6600	432774	4813511	6	90	150	0	0
Fuente de la Salud	IPFS	Santander	4900	432406	4811769	4	71	122	0	0
Gerardo Diego	IPGD	Santander	4900	431469	4811814	353	75	117	0	0
Jesús Cancío	IPJC	Santander	5200	432083	4812077	0	12	61	0	0
José Arce Bodega	IPJA	Santander	5300	434212	4811689	24	154	174	0	0
Magallanes	IPMA	Santander	5850	433879	4812418	18	76	136	0	0
Manuel Cacidedo	IPMC	Santander	6240	430932	4812998	348	168	258	0	0
Manuel Llano	IPML	Santander	5850	432950	4812605	8	132	195	0	0
María Blanchard	IPMB	Santander	7100	435127	4813229	25	112	137	0	0
María Sainz de Sautola	IPMS	Santander	5550	431480	4812376	354	110	265	0	0
Marqués de Estella	IPME	Santander	4300	430340	4810796	336	186	263	0	0
Menéndez Pelayo	IPMP	Santander	6650	435260	4812628	29	89	129	0	0
Nueva Montaña	IPNM	Santander	3150	431590	4809950	351	158	198	0	0
Quinta Porrúa	IPQP	Santander	5700	433098	4812454	10	75	111	0	0
Sardinero	IPSA	Santander	7700	436016	4813420	31	118	282	0	0
Vital Alsar	IPVA	Santander	8800	435496	4814978	22	18	49	0	0
Ramón Pelayo	EPRP	Santander	5350	433450	4812057	15	0	75	0	0
Simón Cabarga	EPSC	Santander	5150	433290	4811905	13	0	77	0	0
Puente III	CCPU	Astillero	1850	433399	4805614	132	65	134	99	0
San José Astillero	CCAS	Astillero	1650	433045	4805554	141	139	308	169	0
Fernando de los Ríos	IPFR	Astillero	2122	433744	4805671	124	143	224	0	0
José Ramón Sánchez	IPJR	Astillero	2000	433270	4805215	142	186	301	0	0
Ramón y Cajal	IPRC	Astillero	2350	430763	4804795	211	157	239	0	0
Altamira	CCAL	Camargo	1500	430598	4806234	248	56	164	106	0

School	Reference	District	Distance from FeMn plant (m)	UTM X (m)	UTM Y (m)	Degrees from FeMn plant	Students 3 - 5	Students 6 - 11	Students 12 – 15	Students 16 -17
Sagrada Familia	CCSF	Camargo	3150	430310	4809494	326	137	320	172	0
Andrés Arche del Valle	EIAA	Camargo	5700	427168	4809825	301	22	0	0	0
Agapito Cagigas	IPAC	Camargo	1800	430404	4806207	248	77	119	0	0
Arenas	IPAR	Camargo	5400	426686	4806046	261	24	32	0	0
Gloria Fuertes	IPGF	Camargo	2250	430903	4808868	331	188	336	0	0
Juan de Herrera	IPJH	Camargo	500	432188	4807348	17	83	254	0	0
Mateo Escagedo Salmón	IPES	Camargo	3600	429400	4809304	313	142	318	0	0
Matilde de la Torre	IPMT	Camargo	850	431252	4807316	301	169	376	0	0
Pedro Velarde	IPPV	Camargo	750	431430	4807365	310	203	325	0	0
Marina de Cudeyo	IPCU	Marina de Cudeyo	7000	438890	4808035	80	126	217	0	0
Bajo Pas	IPBP	Piélagos	8400	423642	4807327	273	174	294	0	0
Eutiquio Ramos	IPER	Piélagos	5900	427640	4802946	228	26	9	0	0
Las Dunas	IPLD	Piélagos	9550	424463	4812666	307	167	342	0	0
Nuestra Señora de Latas	IPSL	Ribamontán al Mar	10500	441179	4812007	60	142	251	0	0
Liceo San Juan de la Canal	CCCL	Santa Cruz de Bezana	8000	427247	4813345	323	29	84	0	0
Buenaventura González	IPBG	Santa Cruz de Bezana	6200	426832	4810241	303	256	450	0	0
José Escandón	IPJE	Santa Cruz de Bezana	7300	427595	4812687	322	213	194	0	0
María Torner	IPTO	Santa Cruz de Bezana	7000	425397	4809110	288	121	146	0	0
Marcial Solana	IPSO	Villaescusa	4700	430515	4802395	198	99	196	0	0
Apostolado del Sagrado Corazón	CCCO	Medio Cudeyo	10500	441773	4802831	112	106	186	0	0
Ave María	CCAM	Medio Cudeyo	9150	440554	4803791	109	11	0	0	0

School	Reference	District	Distance from FeMn plant (m)	UTM X (m)	UTM Y (m)	Degrees from FeMn plant	Students 3 - 5	Students 6 - 11	Students 12 – 15	Students 16 -17
Torreanz	CCTO	Medio Cudeyo	8900	439041	4801404	127	160	324	0	0
Marqués de Valdecilla	IPMV	Medio Cudeyo	8950	440258	4803203	113	179	292	0	0
Alberto Pico	ESAP	Santander	4800	433286	4811534	14	0	0	202	102
Alisal	ESAL	Santander	5400	430730	4812099	346	0	0	176	71
Augusto González de Linares	ESAG	Santander	4150	431138	4810886	347	0	0	216	98
Cantabria	ESCA	Santander	5800	432320	4812633	2	0	0	280	93
José María Pereda	ESJM	Santander	5950	433403	4812650	13	0	0	372	145
La Albericia	ESBE	Santander	5650	431349	4812413	353	0	0	257	184
Las Llamas	ESLL	Santander	7850	435839	4813747	28	0	0	287	257
Leonardo Torres Quevedo	ESTQ	Santander	5050	432276	4811890	2	0	0	350	323
Peñacastillo	ESPE	Santander	4100	430990	4810787	345	0	0	228	86
Santa Clara	ESSC	Santander	6350	434643	4812599	24	0	0	246	495
Villajunco	ESVI	Santander	7600	436108	4813262	32	0	0	310	120
El Astillero	ESAS	El Astillero	2200	433345	4805101	143	0	0	315	148
Nuestra Señora de los Remedios	ESRE	El Astillero	1050	432229	4805830	168	0	0	201	56
Muriendas	ESMU	Camargo	1850	430781	4808212	317	0	0	345	111
Ría del Carmen	ESRC	Camargo	1300	430721	4807070	280	0	0	320	97
Valle de Camargo	ESVC	Camargo	1400	430660	4807133	280	0	0	319	103
Ricardo Bernardo	ESRB	Medio Cudeyo	9000	440185	4803032	115	0	0	422	148
Valle de Piélagos	ESPI	Piélagos	10950	422677	4801078	238	0	0	378	165
La Marina	ESMA	Santa Cruz de Bezana	6200	427067	4810598	307	0	0	357	99

* Consejería de Educación, Cultura y Deporte del Gobierno de Cantabria. Estadística de la Educación en Cantabria. Curso 2015-16. http://www.educantabria.es/ (accessed 10 November 2017)